AIChE WILEY InterScience DISCOVER SOMETHING GREAT

PROCESS SYSTEMS ENGINEERING

Integrated Process and Product Analysis: A Multiscale Approach to Paint Spray

Jia Li, Jie Xiao, and Yinlun Huang
Dept. of Chemical Engineering and Materials Science, Wayne State University, Detroit, MI 48202

Helen H. Lou
Dept. of Chemical Engineering, Lamar University, Beaumont, TX 77710

DOI 10.1002/aic.11311
Published online September 17, 2007 in Wiley InterScience (www.interscience.wiley.com).

It is known that even if process information at macroscale is fully accessible and properly utilized in manufacturing, product and process performance may be still not sufficiently assured. This may be due to the influence of phenomena at finer scales, which are normally not measurable and thus unknown in operation. Besides, even if such information is available, how to integrate it across scales is yet to be discovered. In this work, an integrated process and product analysis methodology is developed via a multiscale approach. This methodology can provide deep understanding of various interrelationships across multiple scales of length and time, which could be essential for substantial improvement of product and process performance. The methodology is successfully applied to the analysis of the paint spray operation in automotive surface coating, with the extension of the analysis from the macroscale of 10^{-2}–10^{1} m and 10^{0}–10^{2} s to the meso-macroscale of 10^{-6}–10^{1} m and 10^{-5}–10^{2} s. Model-based simulation reveals various new opportunities for simultaneous improvement of coating quality, energy and material efficiencies, and environmental cleanness. © 2007 American Institute of Chemical Engineers *AIChE J,* 53: 2841–2857, 2007

Keywords: integrated process and product analysis, multiscale modeling, product quality, energy and material efficiency, environmental quality, automotive paint spray

Introduction

Polymeric material application in vehicle surface coating is technically one of the most challenging tasks in automotive manufacturing. In production, thin films of polymeric materials are built on vehicle surface layer-by-layer through a series of sophisticated, but highly automated operational steps. Because of the lack of real-time information of certain key process and product variables and a possession of insufficient knowledge about the correlation between process operation and product development, coating operational optimality is always a real challenge. This has led to all-time serious concerns of product quality, energy and material efficiencies, VOC emission, and wastewater generation in the industry.

Of the multiple coating layers generated on vehicle surface, the basecoat and clearcoat, known as the topcoat, are most critical to coating appearance and durability. Each of the two layers is developed in two consecutive operational steps: spray and curing. Applying a wet layer of film on a dry layer is known as a "wet-on-dry" procedure. In recent years, a "wet-on-wet" procedure emerges, which asks for an immediate spray of clearcoat on the wet basecoat and let the two layers of wet thin films be baked together. Since the wet-on-wet procedure omits basecoat curing, energy con-

Correspondence concerning this article should be addressed to Prof. Yinlun Huang at yhuang@wayne.edu.

sumption can be reduced and the production rate can be increased. However, this procedure makes quality control more difficult.

In production, vehicle bodies on a conveyor move steadily one-by-one through a spray booth. The booth air condition, such as downdraft air flow, air temperature, and humidity, is set for the effective use of paint material and the cleanness of the work zone. If the design parameters (such as nozzle size and type) are fixed prior to spray, the spray facilities, such as spray bells and robots, still have a number of operating parameters to adjust, such as fluid flow rate, shaping air velocity, and bell voltage and rotation speed. Paint material properties, such as viscosity, temperature, and solid level, are also critical to the final coating quality.

The operational complexity in paint spray is partially reflected by the continuous movement of each vehicle when paint is being applied, and the high production rate. More fundamentally, the lack of online measurements of some key product parameters, such as wet film thickness distribution (i.e., coating topology, macroscopic) and local film behavior (namely surface roughness, mesoscopic), adds additional difficulties in quality control of the production. Note that it is usually required that the dry film thickness deviation (after curing) be less than 10% of the specification. This is basically equivalent to less than 20% of deviation for the wet film (before curing), if the paint solid level is around 50%. Thus, without knowing the wet film thickness and its distribution, an improvement of paint spray operation could be very difficult, if not impossible. On the other hand, surface roughness information (usually for an area less than 10^{-6} m^2 on a panel) can be critical to defect identification and prevention. Hitherto, no technology for online measurement or estimation of such localized film behavior has been reported. Note that without knowing wet film development, the defect-prevention-oriented proactive quality control can be hardly addressed properly. Furthermore, the quality-constrained material and energy efficiency issue cannot be sufficiently addressed, because this relies largely on the knowledge about the relationship between wet-film properties and material/energy use, which is always unknown.

It has been recognized that even if the macroscopic information at the length scale of 10^{-2}–10^{1} m and the time scale of 10^{0}–10^{2} s is fully and properly utilized in process control, it may not be sufficient for achieving some of the production goals, such as high coating quality, low energy and material cost, and/or waste minimization. Product development dynamics and process operation information at the finer scales of length and time (i.e., mesoscale or even microscale) can be critical for product quality assurance and process efficiency improvement. The importance of this type of information to production, however, has not been quite understood. This renders a need of developing wet film modeling methods for characterizing film behavior at the multiscale. Multiscale modeling will facilitate broader and deeper analyses of both process and product and an identification of effective strategies for operational improvement.

Multiscale modeling and simulation has become increasingly attractive over the past decade. A number of general modeling methodologies (e.g., the equation-free approach[1,2] and the heterogeneous multiscale method[3,4]) have been proposed. Most efforts are devoted to developing methodologies applicable for specific engineering applications, including crystallization, plasma spray, hard material, reactor, thermal spray, etc.[5–13] More recently, the issues of process optimization and process control with respect to multiscale objectives have also been investigated.[14–17] These successful investigations have led to various new understandings of the target product and/or process system that are not obtainable using monoscale modeling methods. Needless to say, however, the realm of multiscale modeling and simulation methodologies and technologies needs further exploration. How to describe multiscale phenomena using mathematical language, and how to utilize the information properly in a holistic framework remain as a mountaintop area.

In this article, an integrated process and product analysis (IPPA) framework is developed via a multiscale modeling and simulation approach. The multiscale system models that can characterize simultaneously product and process dynamic behavior at the different spatial and temporal scales enable a comprehensive analysis on the integrated process and product system. Methods on the effective utilization of multiscale information are then presented to derive desirable process-product information at multiple scales. Model-based simulation reveals various usually inconceivable opportunities for simultaneous improvement of product quality, energy and material efficiencies, and cleanness of the work zone. The efficacy of this methodology is demonstrated by a successful application in an automotive paint spray production.

Automotive Paint Spray and Process Modeling

A typical paint spray booth is illustrated in Figure 1, where three bells are mounted above the vehicle pathway and two robots are on each of the two sides of the booth. Vehicles on a conveyor move steadily through the booth one-by-one to get painted. In paint spray, the emulsified paint particles fly at a high speed, and most of them will reach the target vehicle panels. Paint flow rate, shaping air velocity, and electrostatic voltage are among the key spray parameters under control. The booth air temperature and humidity, set based on the paint material used, etc., are critical to the spray operation. The downdraft of the booth provides a balanced top-down airflow profile around the vehicle. An appropriate air flow facilitates paint particles to land on the receiving panels more readily. Those particles unable to reach the panels will be carried by the flow of air to enter the water in drain through the grids on the floor.

Hitherto, most automotive paint spray modeling efforts have been empirical, with coating topology prediction as a major concern. Filev introduced a Jacobian-matrix-based data-driven model to estimate averaged dry film thickness on each panel.[18] The model, which assumes the paint flow rate as the only factor determining film thickness, could be very erroneous in dry film thickness prediction. A neural network (NN)-based paint spray modeling approach introduced by Lou and Huang allows an inclusion of much more input information (including a set of paint spray parameters, booth air parameters, paint property parameters, and vehicle panel and conveyor parameters) for film topology prediction.[19] The

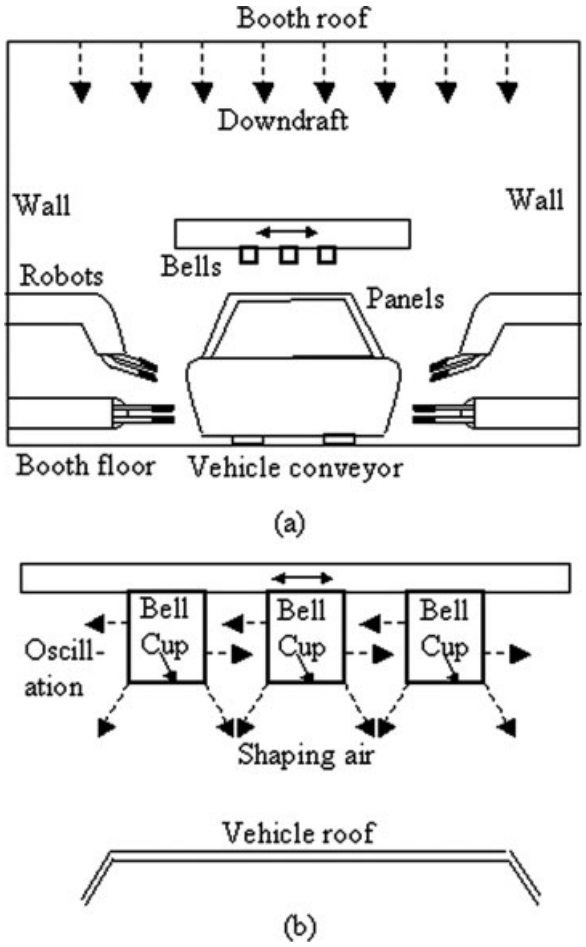

Figure 1. Paint spray booth sketch.

(a) The front view of the spray booth and (b) the close-up view of the region between the bells and the vehicle roof.

model can provide much detailed filmbuild information that is critical to quality prediction and control. Two practical NN models were then developed using industrial data by Zhou and Li.[20,21] However, the prediction of only dry-film topology is a major deficiency of these models. Since the initial wet and the final dry film topologies could be very different, the traditional practice of adjusting spray parameters based on dry film topology may be erroneous.[20]

The other spray process modeling is for predicting coating defects caused by improper spray operation. Lou and Huang developed a defect prediction and analysis model and a defect prevention decision-making algorithm by resorting to artificial intelligence and fuzzy logic techniques.[22] This effort led to successful applications in the analysis of five common types of defects. However, the development of a reliable data-driven model is always restricted by data availability. Note that in real production, it is very difficult, if not impossible, to collect complete, accurate, and sufficient data. It is more difficult to collect data online when a model in application needs to be updated periodically.

Development of first-principles-based spray models is highly desirable, but very challenging. Ellwood and Braslaw developed a finite-element model for an electrostatic spray bell.[23] Although air flow, electric field, and particle trajectories were investigated in detail, the film formation process was not studied. Shah et al. presented numerical simulations for electrostatic powder coating.[24] Gas flow, electric field, and particle trajectories models were utilized to investigate the effects of operational conditions (e.g., powder spray rate, electrostatic voltage, and air flow rate) and particle size change on coating quality (i.e., coating thickness uniformity) and transfer efficiency. The deficiency of the approach is, however, an unrealistic assumption - same particle size from the bell. Colbert and Cairncross studied coating thickness profiles by predicting the trajectories of individual particles between a bell-cup and a receiving panel.[25] An atomization model was involved and different particle size distributions were considered. The known studies provide valuable insights into the paint spray process. However, the known research efforts were restricted to the operation involving only one fixed spray bell and a fixed small receiving plate, which made the study much simpler. Moreover, only a static spray pattern from one bell to a small plate was studied for transfer efficiency investigation. A practical model should be developed using real operating conditions. Paint spray from multiple bells, interaction among bells, enhanced paint particle collision effects due to multiple bell application, synchronized oscillation of bells, receiving panel movement, etc., should all be taken into account. Furthermore, in a comprehensive IPPA, the information at multiple scales of time and length should be utilized appropriately. In addition to coating quality (e.g., coating topology and surface roughness on panels), energy and material efficiency and environmental concerns from the process should also be considered.

Integrated Process and Product Analysis Framework

To identify pathways of achieving multiple objectives in paint spray operation requires an integrated process and product analysis (IPPA), which is based on multiscale characterization for the system. This type of analysis is very challenging since two subtle issues must be appropriately addressed. One issue is about the functionality and applicability of the models that the analysis is based upon. Another issue is about the communication and coordination among the models at the different scales. In this regard, the following tasks need be accomplished before model development: (i) to allocate the scale of each objective, (ii) to identify the relevant process and product variables and their corresponding scales, and (iii) to realize the need for different models.

Scale allocation of objectives

As stated earlier, for a given paint, the operation of paint spray determines coating quality, energy and material use efficiencies, and waste generation from the process (in spray booth, for solvent-borne paint, the dominating environmental concern is VOC emission). Figure 2 provides a multiscale view of how the production objectives are related to process and product parameters as well as material properties.

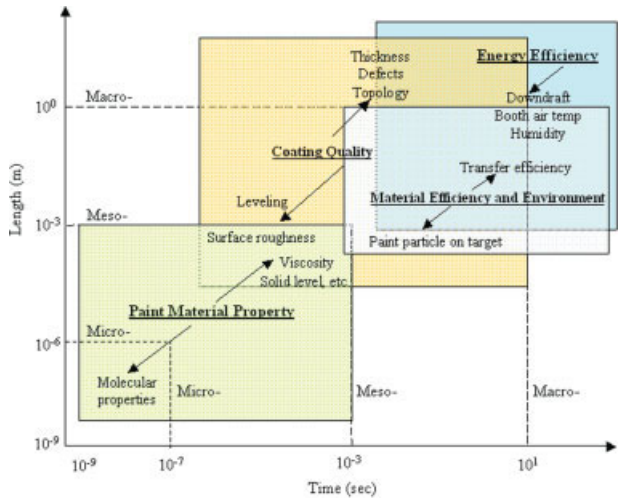

Figure 2. Multiscale analysis of multiobjectives in paint application.

[Color figure can be viewed in the online issue, which is available at www.interscience.wiley.com.]

As shown, energy efficiency improvement is basically a macroscopic issue. The booth air condition is reflected by the settings of downdraft, air temperature, and humidity. These settings determine directly or indirectly energy and material use efficiencies, environmental quality, and coating quality.

Low paint transfer efficiency is equivalent to low material use efficiency and more waste generation. On the other hand, for the same material use efficiency, the paint particles reaching the receiving panels may not land uniformly, which can cause various coating quality problems. The time and length scales in this regard are, to some extent, finer than that for studying energy efficiency.

Coating quality needs to be described in a wider time and length range. Film thickness and uniformity are always measured for each panel, which makes this a macroscopic issue. On the other hand, some types of quality problems are very much localized (e.g., surface roughness, craters, and fish eyes) that need to be studied at the mesoscopic level. Note that in this work, only the panel-based coating topology (or simply coating topology) and localized surface roughness (or simply surface roughness) are studied as the coating quality indicators.

Identification of scale-sensitive process and product variables

Based on the above analysis of production objectives, the process and product variables critical to paint spray can be identified, which are shown in Figure 3. It needs to be pointed out that if paint material properties (e.g., viscosity, and surface tension and its gradient) or paint formulation at the molecular level are considered, the time and length scales will be down to the microscale level. Note that, to simplify the computation work, we assume these paint properties as fixed parameters; thus, the time and length scales in the range of 10^{-9}–10^{-6} are not considered in this work, but this issue will be tackled in future research. Note that Figure 3 embodies Figure 2 by incorporating the following information: (a) the key process and product variables that are symbolized and appeared in the place at appropriate time and length scales, (b) the process and product performance criteria (e.g., energy consumption, transfer efficiency, particle flying time, coating topology, and surface roughness) that are listed in relevant objective blocks, (c) the arrows connecting the variables and related criteria, and (d) the arrows connecting various variables that show the cause–effect relationships useful for model development.

Energy consumption can be characterized by three variables: the air velocity of the downdraft (v_{DD}), the shaping air velocity (v_{SA}), and the applied spray bell voltage (Φ_b). These variables determine the paint spray operation at the macroscopic level. The downdraft airflow is set for making the paint overspray exit from the booth with the exhaust air through the grids on the floor.[26] The shaping air facilitates the atomization of the paint from a bell-cup rotating at a speed of 10–50 kRPM. It shapes paint particles moving toward a receiving panel; otherwise, the particles would primarily leave the bell-cup in the direction perpendicular to the axis of the rotation. The applied bell voltage in the range of 30–90 kV drives the charged paint particles flying to a grounded receiving panel by the coulombic force. By providing higher electrostatic voltage, the coulombic force imposed on particles is accentuated; thereby increasing the paint transfer efficiency.

Paint transfer efficiency and particle flying time can be determined based on particle dynamics at the mesoscopic level, i.e., particle (flying) trajectory $\tilde{z}_i(\tilde{t})$ and particle (flying) velocity $\tilde{\boldsymbol{u}}_i(\tilde{t})$, where the subscript i is the index of each particle. When the particles are sprayed, their velocities and trajectories are controlled by the air drag force (related to the air velocity around the particle, $\tilde{\boldsymbol{v}}_i(\tilde{t})$) and coulombic force (determined by the electric field intensity around the particle, $\tilde{\boldsymbol{E}}_i(\tilde{t})$). By combining them with the particle size information (denoted by the particle diameter, $\tilde{D}_i^p$), the particle distribu-

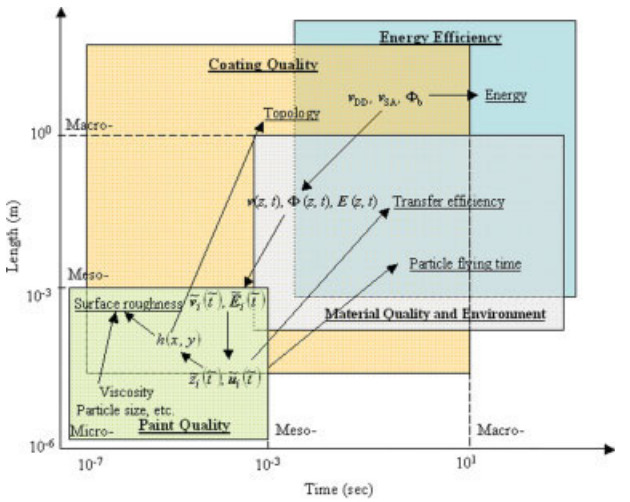

Figure 3. The identification of relevant multiscale process–product parameters.

[Color figure can be viewed in the online issue, which is available at www.interscience.wiley.com.]

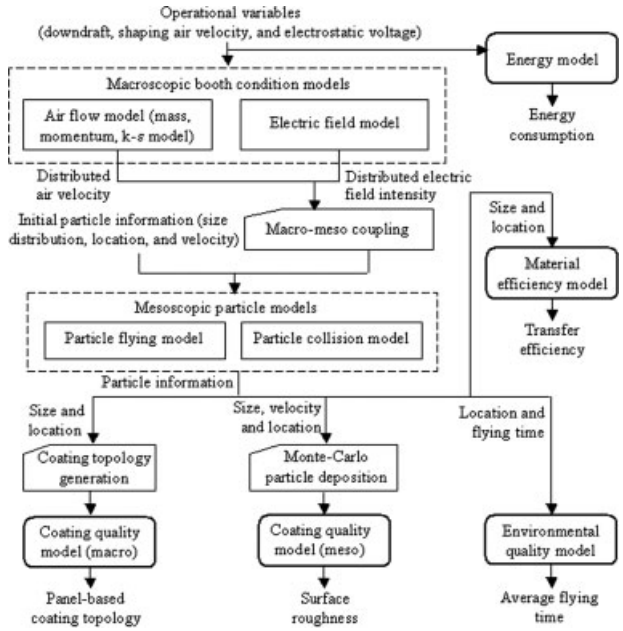

Figure 4. Model framework for IPPA of paint spray.

tion (in flight or on the receiving panel) in terms of size, location, and velocity can be determined.

On the receiving panels, the deposition of particles shapes the film. The deposition process can be characterized by the film thickness information, $h(x,y)$, at different length scales. From the thickness information, mesoscopic surface roughness and macroscopic coating topology can be quantified.

Model needs

The first two steps above suggest that two types of models should be developed for IPPA in paint spray: (i) the multiscale spray system models that reveal the relationship among the process and product variables, and (ii) the performance models that correlate the process-product variables with performances. A complete model framework is shown in Figure 4, which lists all the related models and their connections.

Multiscale Paint Spray Model. The paint spray model consists of two sets of models (see the rectangular boxes in Figure 4): (i) the macroscopic spray booth condition models (i.e., the air flow profile model and the electric field distribution model), and (ii) the mesoscopic particle flying and particle collision models. In addition, three model integration approaches are developed to generate multiple information (see those rectangular boxes with one corner cut in Figure 4): (i) an approach to coupling (macro) continuous phase models with (meso) discrete phase models, (ii) an approach to developing coating topology (macro) from a static spray pattern, and (iii) an approach to generating surface roughness (meso) from a static spray pattern.

In the spray booth, the downdraft velocity, v_{DD}, and the shaping air velocity, v_{SA}, determine the air velocity profile, $\boldsymbol{v}(z, t)$. The bell electrostatic voltage, Φ_b, determines the electric field intensity $\boldsymbol{E}(z, t)$. Here z is the spatial index for the paint booth and t is the time; both are at the macroscopic level. A multiscale strategy is needed to transform the macroscopic information of the operating conditions to the mesoscopic particle-position-based operating conditions, $\tilde{\boldsymbol{v}}_i(\tilde{t})$ and $\tilde{\boldsymbol{E}}_i(\tilde{t})$, which are respectively the air velocity and electric field intensity around particle i at time $\tilde{t}$.

The mesoscopic modeling focuses on the description of the paint particles of microns in size. A particle flying model describes the particle trajectory, $\tilde{z}_i(\tilde{t})$, and the particle flying velocity, $\tilde{\boldsymbol{u}}_i(\tilde{t})$, for a given particle i with diameter $\tilde{D}_i^p$. Since multiple bells are utilized, particle collisions during flying are modeled as well. Note that particle diameter and total particle numbers are changed due to collision.

With the above models, the detailed information of the particles (e.g., sizes, numbers, trajectories, and flying time) can be obtained, and the wet paint film thickness dynamics on the receiving panel can be derived. Note that due to the computational limitation, both the spray bells and receiving panel are set with a fixed location in modeling. Thus, the resultant spray pattern is essentially static. Therefore, an approach is needed to use the static pattern to construct a coating topology by considering spray bell horizontal oscillation and panel movement. On the other hand, surface roughness needs to be generated from the information of the particles constructing that static spray pattern.

Performance Models. The performance models are shown in the rectangular boxes with rounded edges in Figure 4. For paint spray, an energy consumption model can be constructed mainly based on the power used for maintaining the required booth air downdraft. A material efficiency model can be built based on the paint transfer efficiency, which is determined by the final locations and sizes of the particles simulated. An environmental quality model can be created by using the average flying time of the particles unable to land on the receiving panel. The product quality model is established by quantifying macroscopic coating topology and mesoscopic surface roughness. These performance models are all quantified by the related key process and product variables.

Integrated Process and Product Modeling

The automotive paint spray system to be modeled in this study is sketched in Figure 1. For the purpose of demonstrating the modeling methodology, only the paint spray by three bells and the vehicle roof as the receiving panel are considered. As discussed above, IPPA for paint spray needs two types of models, i.e., the multiscale paint spray model and the system performance evaluation model. Each category consists of a number of submodels at different scales as delineated below. Since the models generate the process and product information at multiple scales, methods for communicating and coordinating multiscale information are developed and elaborated as well.

Macroscopic booth condition models

The booth-condition process model set includes a booth air flow profile model and an electric field distribution model; both are at macroscale of time and length.

Table 1. Continuous Phase Air Flow and Electric Field Models

Type	Equation	
Mass conservation[23–25]	$\frac{\partial}{\partial t}\rho_a = -\nabla\cdot(\rho_a \boldsymbol{v}) + S_m$	(T1)
Momentum conservation[23–25]	$\frac{\partial}{\partial t}(\rho_a \boldsymbol{v}) = -\nabla\cdot(\rho_a \boldsymbol{v}\boldsymbol{v}) - \nabla p + \nabla\cdot\boldsymbol{\tau} + \rho_a \mathbf{g} + \sum_i \left\langle \dot{\boldsymbol{S}}_i \right\rangle$	(T2)
	where $\boldsymbol{\tau} = (\mu_a + \mu_t)\left(\nabla\boldsymbol{v} + \nabla\boldsymbol{v}^T\right) - \frac{2}{3}(\mu_a + \mu_t)(\nabla\cdot\boldsymbol{v})\mathbf{I}$	(T3)
	$\mu_t = \rho_a C_\mu \frac{k^2}{\varepsilon}$	(T4)
Standard k-ε turbulence model[23–25]	$\frac{\partial}{\partial t}(\rho_a k) = -\nabla\cdot(\rho_a \boldsymbol{v} k) + \nabla\cdot\left[\left(\mu_a + \frac{\mu_t}{\sigma_k}\right)\nabla k\right] + G_k + G_b - \rho_a\varepsilon - Y_M$	(T5)
	$\frac{\partial}{\partial t}(\rho_a \varepsilon) = -\nabla\cdot(\rho_a \boldsymbol{v}\varepsilon) + \nabla\cdot\left[\left(\mu_a + \frac{\mu_t}{\sigma_\varepsilon}\right)\nabla\varepsilon\right] + C_{1\varepsilon}\frac{\varepsilon}{k}(G_k + C_{3\varepsilon}G_b) - C_{2\varepsilon}\rho_a\frac{\varepsilon^2}{k}$	(T6)
Electric field model [23]	$\nabla^2\Phi(z) = -\frac{\rho^c(z)}{\varepsilon_0}$	(T7)
	$\boldsymbol{E}(z) = -\nabla\Phi(z)$	(T8)
Boundary and initial conditions	$\boldsymbol{v}(z,t) = \begin{cases} \boldsymbol{v}_{SA} & \text{at the bells, } t > 0 \\ \boldsymbol{v}_{DD} & \text{at the booth roof, } t > 0 \\ 0 & \text{at other physical boundaries except floor, } t > 0 \\ 0 & \text{in the spray booth, } t = 0 \end{cases}$	(T9)
	$\Phi(z) = \begin{cases} \Phi_b & \text{at the bells} \\ 0 & \text{on the grounded surfaces} \end{cases}$	(T10)

Booth Air Flow Model. The model can be readily developed by utilizing the well-known conservation equations for mass and momentum, together with the standard k–ε turbulence model (see Eqs. T1–T6 in Table 1).[23–25] Note that the air in the spray booth is assumed to be static initially, then fresh air begins blowing downward from the booth ceiling. The air flow is interfered by the shaping air flow near the spray bells. Finally, the exhaust air flows out of the spray booth through the grids on the floor. These define the initial and boundary settings for the air velocity (see Eq. T9 in Table 1).

Electric Field Model. Ellwood and Braslaw introduced an electric field model, which consists of a Poisson equation and a correlation between the electric field intensity and electrostatic potential.[23] The model is listed in Table 1 (Eqs. T7 and T8). Note that the electrostatic potential is not a function of time, since a pseudo-steady-state approximation for the electric field is assumed, which means the potential reacts instantaneously to any changes in the charge density.[23] The electrostatic potential at the bell-cup and grounded substrates (i.e., the walls of the spray booth and the vehicle panels) are imposed as boundary conditions (Eq. T10 in Table 1). This model describes the physics of a high negative voltage application to the emitting electrode at the bells, which generates an electric field between the bells and the grounded surfaces.

Mesoscopic particle models

Three mesoscopic particle models are needed to identify correlation between the booth conditions and the particle dynamics. Note that the dynamics is described at the mesoscopic level due to particle size in micron.

Particle Flying Model. It is assumed that spherical paint particles with the same density are delivered from the spray nozzle, and the momentum of particles is affected by only three dominant forces: the drag force from the surrounding turbulent air flow, the electrical force from the electric field, and the gravity. Based on these assumptions, the velocity of each particle ($\tilde{\boldsymbol{u}}_i$), individually labeled by subscript i, can be modeled based on Newton's second law of motion (Eqs. T11–T14 in Table 2).[25,27] The initial particle velocities chosen in this model have the magnitude of u_0 and the direction of θ angle away from the axis of the cylindrical bell (Eq. T16). The initial particle size distribution is assumed to be a lognormal distribution (Eq. T17).[25]

Particle Trajectory Model. The particle trajectory ($\tilde{\boldsymbol{z}}_i(\tilde{t})$) can be readily determined by applying Eq. T15 in Table 2 when the particle velocity ($\tilde{\boldsymbol{u}}_i(\tilde{t})$) and particle initial locations

Table 2. Discrete Phase Particle Models

Type	Equation
Particle flying model[25,27]	$\frac{d\tilde{\boldsymbol{u}}_i(\tilde{t})}{d\tilde{t}} = \frac{3\pi\mu_a\tilde{D}_i^p}{\tilde{m}_i}(\tilde{\boldsymbol{v}}_i(\tilde{t}) - \tilde{\boldsymbol{u}}_i(\tilde{t}))f_i + \frac{\tilde{q}_i}{\tilde{m}_i}\tilde{\boldsymbol{E}}_i(\tilde{t}) + \mathbf{g}$ (T11)
	where $\tilde{m}_i = \frac{1}{6}\pi(\tilde{D}_i^p)^3\rho_p$ (T12)
	$f_i = \begin{cases} 1 + \frac{(\mathrm{Re}_i^r)^{2/3}}{6}, & \mathrm{Re}_i^r < 1{,}000 \\ 0.0183\,\mathrm{Re}_i^r, & 1{,}000 \le \mathrm{Re}_i^r < 3\times 10^5 \end{cases}$ (T13)
	$\mathrm{Re}_i^r = \frac{\tilde{D}_i^p\lvert\tilde{\boldsymbol{v}}_i(\tilde{t}) - \tilde{\boldsymbol{u}}_i(\tilde{t})\rvert\rho_a}{\mu_a}$ (T14)
Particle trajectory model[25]	$\frac{d\tilde{\boldsymbol{z}}_i(\tilde{t})}{d\tilde{t}} = \tilde{\boldsymbol{u}}_i(\tilde{t})$ (T15)
Initial conditions	$\tilde{\boldsymbol{u}}_i(0) = \boldsymbol{u}_0$ (T16)
	$f(\tilde{D}^p;\mu,\sigma) = \frac{1}{\sqrt{2\pi}\sigma\tilde{D}_p} \times\exp\left[-\frac{(\ln\tilde{D}_p - \mu)^2}{2\sigma^2}\right]$ (T17)
	$\tilde{\boldsymbol{z}}_i(0) = \boldsymbol{z}_{i0}$ (T18)
Particle collision model[29]	$P_{i,j} = \frac{\pi\left(\tilde{D}_i^P + \tilde{D}_j^P\right)^2\lvert\tilde{\boldsymbol{v}}_i(\tilde{t}) - \tilde{\boldsymbol{v}}_j(\tilde{t})\rvert\Delta\tilde{t}}{4V_{cell}}$ (T19)

are known. The initial positions of particles are assumed uniformly distributed around the annulus of the bell-cup lip (Eq. T18).

Particle Collision Model. Gavaises et al. have proved that particle collisions, especially in the multiple bells application cases, have a great influence on particle size and, as a consequence, on particle velocities and trajectories.[28] In this work, O'Rourke's collision algorithm, which uses statistical approaches, is applied to determine particle collisions.[29] It is assumed that there is a probability of any particle colliding with any other particle given by Eq. T19 in Table 2. The detailed model information can be found in O'Rourke (1981).[29]

Performance models

The integrated process and product model can provide the information necessary for evaluating system performance in terms of energy consumption, paint transfer efficiency, booth environmental cleanness, and coating topology and surface roughness. The performance assessment models are described below.

Energy Consumption. In spray operation, energy is consumed by the fans that provide booth air downdraft and by the spray facilities that generate shaping air and electric field. Industrial practice shows that the power needed for maintaining downdraft is much beyond that for the other two. According to Perry and Green, the power for the fans (E_d) is proportional to the downdraft air flow velocity ($\boldsymbol{v}_{DD}$) as follows,[30]

$$E_d = c\boldsymbol{v}_{DD} \tag{1}$$

where c is a coefficient.

Paint Transfer Efficiency. The transfer efficiency (TE) is defined as the ratio of the amount of paint received by the panels over the total amount of paint delivered by the spray facilities. If the mass of paint is counted by the mass of the particles involved, then a TE expression can be simplified as the one using the diameter of each particle, $\tilde{D}_i^p$; this gives

$$\mathrm{TE} = \sum_i^{N_p}(\tilde{D}_i^p)^3 \Big/ \sum_j^{N_b}(\tilde{D}_j^p)^3 \tag{2}$$

where N_p and N_b are the total number of particles landed on the panel surface and that from the bells, respectively.

Booth Air Quality. During paint spray, particles reach their destinations (i.e., panel surface, booth wall or floor) at different time instants. The particle concentration in the air reflects booth air quality.[31] It is very difficult to know the exact number of particles at any time instant. An alternative way is to estimate the particles' average flying time (AFT). A longer AFT indicates an increase of particle concentration in the air and thus more VOC release to the booth. A reasonable estimation of AFT is to count those particles not landing on the receiving panels.

Let $\tilde{t}_{0_i}$ and $\tilde{t}_{f_i}$ be, respectively, the time of the ith particle leaving a spray facility and the time of the same particle landing on a panel or the booth floor. AFT can be identified as the mean value of the flying time of particles not landing on the receiving panels.

$$\mathrm{AFT} = \underset{\tilde{z}_i\notin\text{panel}}{\mathrm{Avg}}\,(\tilde{t}_{f_i} - \tilde{t}_{0_i}) \tag{3}$$

where $\tilde{z}_i$ is the final position of particle i from a spray facility.

Coating Topology. Coating topology can be depicted graphically through simulation, which gives a complete view of the entire panel. In industry, film topology is reflected by measuring the film thickness of a limited number of locations on a panel of a sampled vehicle. For a roof panel, for instance, the film thickness in three rows (front, middle, and rear) are measured; each row may have 8–10 equally distanced locations. Then the thickness data collected from each row is plotted to show the thickness uniformity. Apparently, a larger difference of the thickness at each pair of adjacent locations indicates a poorer coating topology. Based on this, a topology quality indicator can be created, which is the mean gradient of the thickness of the adjacent measurement locations throughout the panel, i.e.,

$$H_{pt} = \frac{1}{N_{pt}(M_{pt}-1)}\sum_{i=1}^{N_{pt}}\sum_{j=2}^{M_{pt}}\frac{\lvert h_{i,j} - h_{i,j-1}\rvert}{\Delta x} \tag{4}$$

where $h_{i,j}$ is the film thickness at the jth location of the ith row on the panel, Δx is the distance between the two adjacent measurement locations in the same row, and N_{pt} and

M_{pt} are, respectively, the total number of rows and the number of locations in each row. This indicator unveils the severity of thickness changes in both magnitude and frequency. A uniform coating gives the minimum topology indicator value (i.e., zero), while a larger value indicates a less smooth coating surface.

Surface Roughness. A common approach to quantifying surface roughness is to evaluate the standard deviation.[13] In this study, surface roughness (H_{sr}) is studied for any area of 10^{-6} m^2 on the panel. In the modeling work, each target area is divided into $N_{sr} \times M_{sr}$ grids, and the film thickness ($h_{i,j}$) at the location of each grid point is evaluated. These estimations are compared with their average thickness ($\overline{h}$) of the target area. This gives the following formula:

$$H_{sr} = \sqrt{\frac{1}{N_{sr} \times M_{sr}} \sum_{i}^{N_{sr}} \sum_{j}^{M_{sr}} (h_{i,j} - \overline{h})^2} \tag{5}$$

Methods for communicating and coordinating multiscale information

The models listed in Tables 1 and 2 describe various types of phenomena occurring at different time/length scales. Thus, multiscale model integration approaches are needed to effectively utilize the information generated from the models. The approach should be capable of handling: (i) the utilization of air flow and electric field information at the macroscopic level (booth air profile and electric field profile based, which is continuous) to the particle information at the mesoscopic level (particle-position-based, which is discrete), (ii) the generation of coating topology (macroscale) from a static paint spray pattern, and (iii) the development of surface roughness information (mesoscale) by utilizing the macroscopic particle distribution information.

Macro (Continuous Phase)–Meso (Discrete Phase) Coupling. The air flow model, the electric field model, and the particle models are all coupled, but the coupling is assumed weak enough that each can be calculated separately as shown in Figure 4. Because the momentum exchange between the (discrete) particles and the (continuous) gas phase is negligible (i.e., $\langle \dot{\boldsymbol{S}}_i \rangle$ in Eq. T2 equals zero) and the evaporation of the solvent of paint particles can be safely neglected (S_m in Eq. T1 equals zero), coupling between the air flow field and the particle dynamics is one-way and the air flow field can be predicted first.[23,25] The interaction between the electric field and the particle dynamics is also simplified by neglecting the influence of charged particles on the electric field.[27,32,33] Consequently, Laplace's equation (ρ^c equals zero in Eq. T7) is used to determine the electric field before particle trajectory calculation.

With these simplifications, in continuous-phase simulation, the distributed air flow and electric field information (i.e., the information at every mesh point) can be calculated numerically by a computational fluid dynamics (CFD) solver. The resolution of the results depends on the size of the simulation cells (10^{-2}–10^{-1} m) of the spray booth, which are at the macroscopic level. The particle flying model needs the particle-position-specific information about the air velocity and the electric field intensity, which has the same length scale as the particle size (10^{-6}–10^{-5} m), which is at the mesoscopic level. To utilize the information across these length scales, a linear interpolation approach is applied in the spatial domain. By knowing the particle location, $\tilde{z}_i$, at time $\tilde{t}$, the particle-based air velocity, $\tilde{\boldsymbol{v}}_i(\tilde{t})$, and the electric field intensity, $\tilde{\boldsymbol{E}}_i(\tilde{t})$, can be obtained based on their values at the nearest cell nodes.

$$\tilde{\boldsymbol{v}}_i(\tilde{t}) = \boldsymbol{v}(z,t) + \frac{\boldsymbol{v}(z+\Delta z,t) - \boldsymbol{v}(z,t)}{\Delta z}(\tilde{z}_i(\tilde{t}) - z) \tag{6}$$

$$\tilde{\boldsymbol{E}}_i(\tilde{t}) = \boldsymbol{E}(z,t) + \frac{\boldsymbol{E}(z+\Delta z,t) - \boldsymbol{E}(z,t)}{\Delta z}(\tilde{z}_i(\tilde{t}) - z) \tag{7}$$

where $\tilde{z}_i(\tilde{t}) \in [z, z+\Delta z)$ and $\tilde{t} \in [t, t+\Delta t)$. Note that the time domain is not involved in the interpolation. This attributes to a small difference of macroscopic values between each adjacent time step, which can be assumed to be negligible in interpolation. Also note that, in modeling, when the mesh size for simulation and the total number of paint particles are determined, the system's degree of freedom is determined.

Coating Topology Generation. The other type of integration focuses on the paint film development on the entire panel by utilizing the information from the static spray pattern in a specific panel location. Note that the particle flying model provides a way to trace every particle's behavior from the bells to a receiving panel or otherwise the surrounding (i.e., the booth environment and the booth floor). Thus, the particle distribution information can be obtained by recording the particle properties in every specific landing location of the receiving panel. The particle distribution in terms of size, velocity, and location is the key factor to coating quality estimation.

A real paint application process is complicated, where each vehicle body moves at a certain line speed and the bells above the roof move horizontally with a certain frequency and amplitude in the direction perpendicular to the vehicle movement. For the given spray bell operational setting, the number of paint particles from each bell per second could be in the order of 10^9. Thus, to paint a roof of 1.3×1.8 m^2 by three bells within 27 s, for example, the total number of particles sprayed could be in the order of 10^{11}. Note that in model-based simulation, particle collision and spray bell oscillation must be considered to have a better approximation of real operation. With these considerations, it is impractical to simulate the particles in the order of 10^{11} directly for a multiple-bell operation when studying the generation of a coating layer of about 70 μm on a panel.

When the panel surface to be painted is planar and the relative orientation of the bell to the surface is not changing, the difference of the spray patterns due to the bell movement can be reasonably neglected, which means the static spray pattern at any moment of operation is nearly identical, or the difference of the patterns obtained in different time instants is negligible in studying coating topology.[34–36] Under this assumption, it should be appropriate to use the paint-spray (mesoscopic) information obtained from a static spray pattern (i.e., simulation based on the fixed locations of bells and receiving panels) repeatedly in a constructive way to generate a coating layer (macroscopic) on the panel. This allows the use of a superposition approach to add the particle static

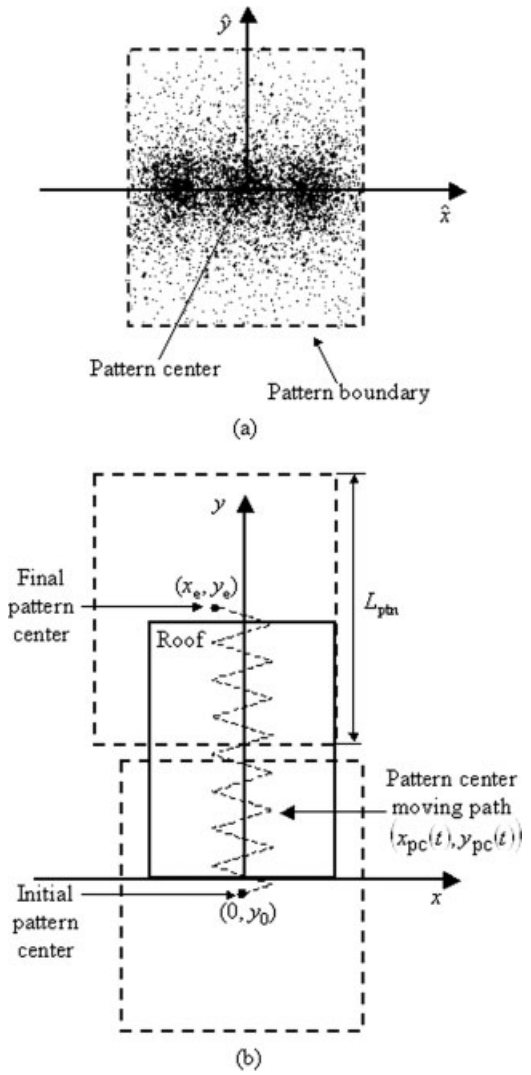

Figure 5. Film topology generation from the static spray pattern.

(a) A static spray pattern generated by three bells and (b) illustration of pattern center migration.

patterns in the pathway that bell movement follows. A procedure using this approach is delineated below.

Step 1. Calculate the static film growth (SFG) rate. The static spray pattern shown in Figure 5a provides the detailed information of the landed particles (i.e., the locations and sizes). The area covered by the spray pattern on a receiving panel needs to be divided into N_{cell} cells. The total volume of particles landing on any jth cell (denoted as cell_j) is assumed to spread over the area of the cell, and the deposition of the particles causes the growth of the film thickness. The particles landing on the edges of the cell can be randomly assigned to one of the adjacent cells sharing that edge. The SFG rate in cell_j is calculated by dividing the thickness of cell_j by the particle generation time, i.e.,

$$\delta_{\text{cell}_j} = \frac{\sum_{(\hat{x}_i,\hat{y}_i)\in \text{cell}_j} \pi(\tilde{D}_i^{\text{P}})^3}{6A_{\text{cell}_j} t_{\text{r}}} \qquad j = 1, \ldots, N_{\text{cell}} \tag{8}$$

where $(\hat{x}_i, \hat{y}_i)$ is the location of the ith particle in the static pattern, $\tilde{D}_i^{\text{P}}$ is the diameter of the ith particle, $A_{\text{cell}j}$ is the area of cell_j, and t_{r} is the time needed for the bells to deliver the number of particles used in simulation. It is assumed that at any location in cell_j, the SFG rate is identical, i.e.,

$$\delta(\hat{x}, \hat{y}) = \delta_{\text{cell}_j}, \quad \text{if } (\hat{x}, \hat{y}) \in \text{cell}_j \tag{9}$$

where $\delta(\hat{x}, \hat{y})$ is the SFG rate at location $(\hat{x}, \hat{y})$.

Step 2. Calculate the trajectory of the pattern center. Without considering any unknown disturbances, the same static pattern is assumed to be applicable throughout the paint spray operation. The coating topology generation is illustrated in Figure 5b, where the roof is assumed in a fixed location, while the static pattern (the area defined by dashed lines) moves continuously by following the path specified by the saw-shaped curve that is described by the x–y coordinate (x is the direction of bell movement, and y is the direction of vehicle movement). This means that the relative motions of the spray bells to the vehicle body are observed. In other words, the motions of the spray bells are observed by following the vehicle body (i.e., a Lagrangian view). Note that using a Lagrangian reference frame or an Eulerian reference frame will give the same trajectory of the pattern center on the vehicle roof. The static pattern moves from the initial location (i.e., the panel starts to be painted and the pattern center is at $(0, y_0)$) to the final location (i.e., the panel just finishes painting and the pattern center is at $(x_{\text{e}}, y_{\text{e}})$). Note that the saw-shaped curve is the trajectory of the pattern center [i.e., $(x_{\text{pc}}(t), y_{\text{pc}}(t))$] and it can be determined by the bell oscillation speed v_{b} and the conveyor line speed v_{c} as follows:

$$x_{\text{pc}}(t) = \begin{cases} \beta L_{\text{a}} & 0 \le \beta < 1 \\ L_{\text{a}} - (\beta - 1)L_{\text{a}} & 1 \le \beta < 2 \\ -(\beta - 2)L_{\text{a}} & 2 \le \beta < 3 \\ -L_{\text{a}} + (\beta - 3)L_{\text{a}} & 3 \le \beta < 4 \end{cases} \tag{10}$$

$$y_{\text{pc}}(t) = y_0 + v_{\text{c}} t \tag{11}$$

where L_{a} is the amplitude of the bell oscillation (i.e., the maximum distance that the bell moves away from the equilibrium position). Assuming that the bells begin to move from the equilibrium positions, β can be calculated as:

$$\beta = \text{mod}\left(\frac{v_{\text{b}} t}{L_{\text{a}}}, 4\right) \tag{12}$$

where mod is an operator that gives the remainder after dividing two values in the parenthesis. The term, $v_{\text{b}}t/L_{\text{a}}$, is the number of amplitudes that the bell has traveled. Note that traveling four amplitudes is one oscillation cycle and β always differs from $(v_{\text{b}}t/L_{\text{a}})$ by a multiple of 4.

Step 3. Calculate the coating topology. In this process, the accumulated film thickness at any location [e.g., Location A having coordinates (x_A, y_A)] on the roof can be calculated by integrating film growth rate over a certain time period. Note that the film spreading during paint spray does affect

the film roughness (in the length scale of 10^{-4}–10^{-3} m), but not the film topology (in the length scale of 10^{-1}–10^{0} m) due to the high viscosity of the paint material. Thus, the thickness at Location A can be derived as

$$h(x_A, y_A) = \int_{t_A^0}^{t_A^e} \delta(\hat{x}_A(t), \hat{y}_A(t))dt \tag{13}$$

where $h(x_A, y_A)$ is the film thickness at Location A. t_A^0 is the time when Location A starts to be painted (i.e., when the static pattern starts touching this location) and t_A^e is the time when Location A just finishes painting (i.e., when the static pattern just leaves this location); they are given by

$$t_A^0 = \max\left\{\frac{2y_A - L_{\text{ptn}} - 2y_0}{2v_c}, 0\right\} \tag{14}$$

$$t_A^e = \min\left\{\frac{2y_A + L_{\text{ptn}} - 2y_0}{2v_c}, \frac{y_e - y_0}{v_c}\right\} \tag{15}$$

where L_{ptn} is the pattern length in the $\hat{y}$ direction (see Figure 5). Note that the time when the panel begins to be painted is 0 and the time when the panel just finishes painting is $(y_e - y_0)/v_c$, which become, respectively, lower and upper boundaries for t_A^0 and t_A^e.

Variable $\delta(\hat{x}_A(t), \hat{y}_A(t))$ is the film growth rate for Location A on the roof at time t (it is also the SFG rate at location $(\hat{x}_A(t), \hat{y}_A(t))$ in the static pattern). Note that $(\hat{x}_A(t), \hat{y}_A(t))$ is the location on the static pattern overlapped with Location A on the roof at time t. Since axes x and y are fixed, while axes $\hat{x}$, $\hat{y}$ move along with the static pattern, although Location A on the roof is fixed, location $(\hat{x}_A(t), \hat{y}_A(t))$ in the static pattern continuously changes with time, which means the film growth rate for Location A on the panel changes with time. Since the pattern center is always at the origin of $\hat{x}-\hat{y}$ coordinate, location $(\hat{x}_A(t), \hat{y}_A(t))$ can be derived as:

$$\hat{x}_A(t) = x_A - x_{\text{pc}}(t) \tag{16}$$

$$\hat{y}_A(t) = y_A - y_{\text{pc}}(t) \tag{17}$$

Since A is any location on the roof, a film topology can be obtained in this way.

Mesoscopic Surface Roughness Generation. Surface roughness refers to the surface topological behavior in a very small area (e.g., 10^{-6} m^2) on the receiving panel. In such an area, paint film is developed with a chaotic growth of flat cylinders formed by the splashing of spherical particles onto the receiving panel. Obviously, no film microstructures will be identical. It is, therefore, necessary to perform random simulation many times to obtain valid statistical averages of the properties for a given operating condition.[13] With the assumption that the distributions of particle size and velocity at any localized area are consistent with the one collected from the static spray pattern, a rule-based Monte Carlo method is employed to explore the particle deposition process by following the steps below.

Step 1. Generate a complete list of the particle information (sizes and velocities) from the static paint spray pattern (see example in Figure 5a).

Step 2. Select a particle randomly from the list, and specify randomly the particle landing position (x_{0i}, y_{0i}) in the area of study.

Step 3. Convert the particle from its spherical shape to a cylindrical shape. Because of the high viscosity and low surface tension of the paint material, it is appropriate to assume that each particle can be approximated by a cylindrical splat after splashing.[37] The cylinder diameter $(\tilde{D}_i^s)$ is a function of the particle diameter $(\tilde{D}_i^p)$, velocity $(\tilde{u}_i)$, paint density (ρ_p), and paint viscosity (μ_p) as follows[38]:

$$\tilde{D}_i^s = 2\tilde{D}_i^p \left(\frac{\rho_p \tilde{u}_i \tilde{D}_i^p}{\mu_p}\right)^{0.2} \tag{18}$$

Correspondingly, the height $(\tilde{h}_i^s)$ of the splat can be calculated as below:

$$\tilde{h}_i^s = \frac{2\left(\tilde{D}_i^p\right)^3}{3\left(\tilde{D}_i^s\right)^2} \tag{19}$$

Step 4. If the landing location can accommodate the cylindrical splat, the splat keeps the same shape (see Figure 6a); otherwise, its shape is modified to conform to the surface under it, while keeping its height the same (see Figure 6b). The film thickness in the area covered by the splat or modified splat is then updated by adding the height of splat to the thickness of the existing coating (see Figure 6), i.e.,

$$h(x,y) = \begin{cases} h_0(x,y) + \tilde{h}_i^s, & \text{if } ||(x,y) - (x_{0_i}, y_{0_i})|| \le \frac{\tilde{D}_i^s}{2} \\ h_0(x,y), & \text{otherwise} \end{cases} \tag{20}$$

where $h_0(x,y)$ is the current film thickness at location (x,y), and $||(x,y) - (x_{0i}, y_{0i})||$ gives the distance between the studied location (x,y) and the particle landing location (x_{0i}, y_{0i}).

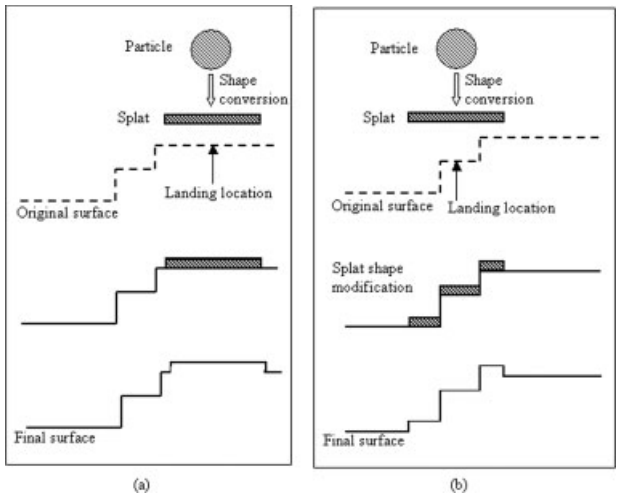

Figure 6. Illustration of particle deposition and coating thickness growth.

(a) Without splat shape modification and (b) with splat shape modification.

Table 3. Process and Product Parameter Specifications

Parameters		Base Case Value
Geometry parameter	Spray booth geometry	$13.5 \times 8.0 \times 4.9$ m^3
	Roof width	1.3 m
	Roof length	1.8 m
	Distance from bell to roof	0.254 m
	Distance between two adjacent bells	0.45 m
	Bell diameter	0.057 m
Process operating condition	Bell oscillation period	3.6 s/cycle
	Bell oscillation amplitude	0.2 m
	Bell rotational speed	40,000 rpm
	Applied voltage	70 kV
	Paint flow rate	1.75×10^{-6} m^3/s
	Shaping air initial velocity	15 m/s
	Downdraft air initial velocity	0.5 m/s
	Conveyer speed	0.067 m/s
Material-related parameter	Paint density	1.2 g/cm^3
	Paint viscosity	0.01 Pa·s
Others	Charge per unit mass	2.8 μC/g
	Coefficient in the energy equation	17.9 kW/m/s

Step 5. Evaluate the averaged film thickness of the target area. If it reaches the anticipated thickness, go to Step 6; otherwise, return to Step 2.

Step 6. Output the surface roughness information that is described by the function,

$$h(x, y) = \{h(x_i, y_i) | (x_i, y_i) \in A_{sr}\}, \tag{21}$$

where A_{sr} is the studied small area, and (x_i, y_i) are the selected locations in this area.

Simulation and Analysis

Application of the introduced IPPA approach is illustrated through studying an automotive clearcoat spray system that is depicted in Figure 1, with the focus on the roof panel. The geometries of a spray booth, vehicle panel, and spray bells, the normal operating conditions and paint material properties resemble practical industrial data. The ratio of particle charge to mass (see coefficient of the electric field intensity term of Eq. T11 in Table 2) is assumed constant according to Ellwood and Braslaw.[23] Table 3 lists the parameters used as the base case settings in simulation. Parametric studies are performed by varying some operating conditions.

In each simulation run, around 10,000 particles with a specified lognormal particle size distribution are simultaneously sprayed out from three bells. The moving trajectories of these particles are tracked in simulation. Note that due to the consideration of particle collision during spray, the total number of particles and particle sizes change along time. Considering the trade-off between computational cost and results quality, the finite element meshes used for calculating air flow and electric field in the booth are made up of more than 10^6 irregular triangular cells with the length scale of 10^{-2} m.[27,39]

Base case study

A total of ~10,000 particles with 21 different sizes distributed (lognormal) in the range of 2–42 μm are sprayed from the bells simultaneously. According to the atomization model provided by Bell and Hochberg,[40] the mean particle diameter ($\overline{\tilde{D}}^p$) is determined based on the bell voltage (Φ_b), rotational speed (ω), paint flow rate (V_L), and paint viscosity (μ_p) as follows:

$$\overline{\tilde{D}}^p = C\Phi_b^{-0.2}\omega^{-0.7}V_L^{0.4}\mu_p^{-0.2} \tag{22}$$

where C is a dimensionless atomization constant. Using the settings in Table 3 and a C value of 4,300, the mean particle diameter ($\overline{\tilde{D}}^p$) is 11.3 μm.

Spray Booth Condition and Particle Flying Information. The air velocity profile, electric field profile, and particle flying time distribution are shown in Figure 7. Particles will reach physical boundaries (e.g., the receiving panels, and spray booth walls and floor). The detailed particle information (i.e., location, size, velocity, and the flying time from the bell to the boundary) will be recorded for analysis.

Spray Pattern Analysis. In the static spray pattern shown in Figure 8, the small black dots represent the particles; the size of each dot is plotted proportional to the size of the real particle. It is understandable that, dense clouds are formed directly beneath the bells while other regions have lower particle densities. This indicates that three "hills" of the film will be formed on the received panel at the location directly beneath the three bells. It can be anticipated that the bell oscillation during spray will help in achieving film topology uniformity. Note that although the width of the roof is only 1.3 m, a complete static spray pattern (i.e., the area bounded by the dashed rectangle in Figure 8) spanning 1.7 m in the $\hat{x}$ direction is obtained, because the bells oscillate in x direction with an amplitude of 0.2 m (see an illustration in Figure 5). The pattern spans 2 m in the $\hat{y}$ direction, so that 99.62% of the total volume of particles landing on the receiving panel is included in this pattern. This pattern is used for film topology generation.

Particle Size Distribution in the Static Pattern. This information is essential for estimating surface roughness. Figure 9 gives the particle size distribution on the receiving panel (denoted by bars). Note that the particle size is represented by the particle diameter. Initially, 9,973 particles with 21 different initial size ranging from 2 to 42 μm are sprayed out of the three bells. The number of particles for each size class is shown by "o" in the figure. The particle size distribution on the receiving panel is also shown in the same figure by those bars, each of which gives the number of particles in a certain diameter range. Note that after traveling, the total number of particles is decreased by 28% (from 9,973 to 7,189) due to particle collision. Among those 7,189 particles, 5,704 particles land on the receiving panel and the static spray pattern is formed. In this pattern, there are 2,467 different particle sizes ranging from 2 to 52.7 μm. The noticeable decrease in the total number of particles, a significant increase in the number of particle size classes (i.e., from

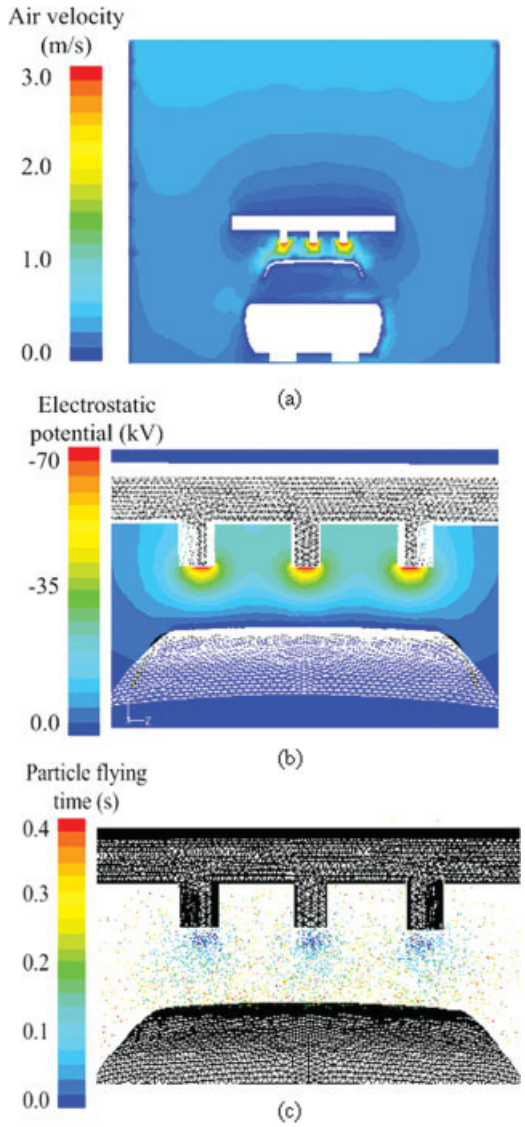

Figure 7. Simulation results of spray booth condition and particle flying.

(a) Air velocity profile, (b) electric field profile, and (c) particle flying time profile. [Color figure can be viewed in the online issue, which is available at www.interscience.wiley.com.]

21 to 2,467), and the broadened particle size ranges indicate the significance of collision effects, especially for the multiple bell case studied in this work. Comparing the size distribution of particles just out of the bells (namely "initial distribution") with that on the receiving panel, it appears that the curve of particle size distribution on the panel is shifted to the right side slightly. This is because: (i) the collided particles may merge into new particles with larger sizes, and (ii) larger particles have a greater momentum, thus they have a higher probability of reaching the receiving panel while smaller particles tend to fly around in the turbulent air.

Performance Evaluation. This evaluation focuses on coating quality, energy consumption, material use efficiency, and booth air quality.

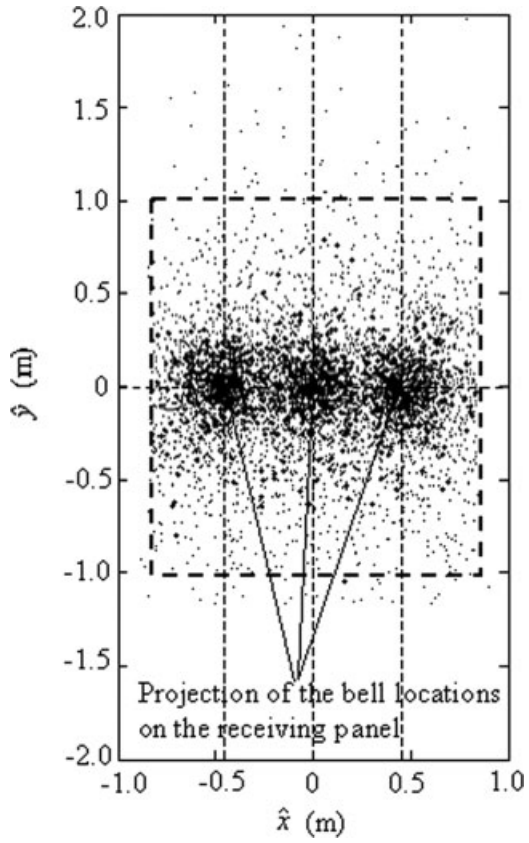

Figure 8. Static spray pattern in the base case.

Based on the static spray pattern in Figure 8, the SFG rate and the coating topology can be readily derived by following the procedure presented in the modeling part. The film topology on the roof is shown in Figure 10b, and the film thickness distribution in 10 selected locations is plotted in Figure 11. These locations are uniformly distributed in each of three selected rows (parallel to the x direction): the front row (y =

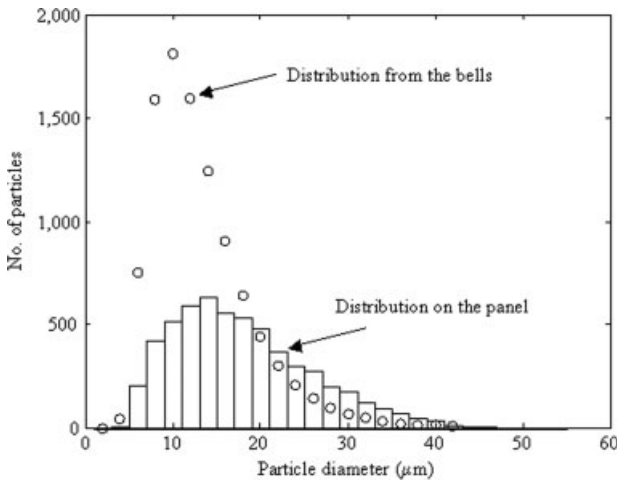

Figure 9. Particle size distribution in the base case.

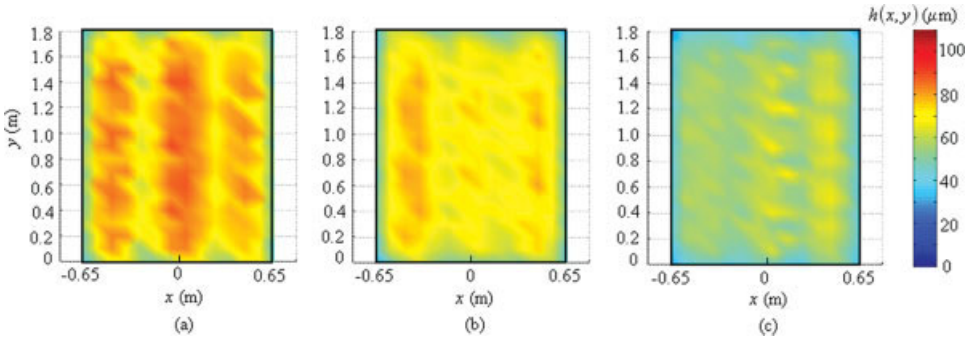

Figure 10. Panel-based coating topology under different initial particle size distributions (three mean diameters).

(a) 16.9 μm, (b) 11.3 μm (base case), and (c) 7.6 μm. [Color figure can be viewed in the online issue, which is available at www.interscience.wiley.com.]

0.3 m), the center row (y = 0.9 m), and the rear row (y = 1.5 m). This type of coating topology and thickness representation is commonly practiced in industry. As shown in Figure 11, both the mean and the standard deviation of film thickness indicate that the wet clearcoat topology and thickness are quite acceptable. Note that due to the consideration of turbulent air flow in the particle flying simulation, the static spray pattern may not be symmetric. In this case study, the left side of the static spray pattern has a smaller static film growth (SFG) rate than the right side. This static spray pattern was utilized repeatedly to generate a coating layer. As a result, it gives a persistent dip on the left side (see Figure 11). Because of various limitations, only the mean film thickness and the coating topology are quantified for coating quality evaluation.

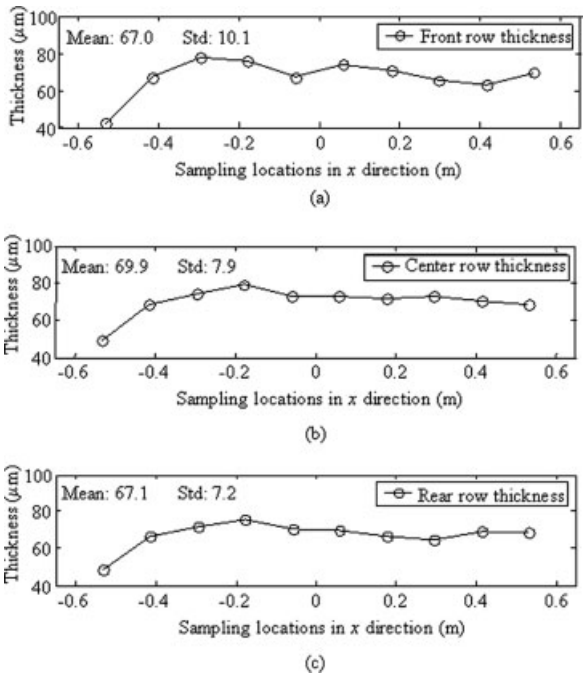

Figure 11. Film thickness at the sampling locations on the panel in the base case.

(a) Front row, (b) center row, and (c) rear row.

In the mesoscopic scale, coating topology provides only mean thickness information in a localized area (i.e., 1 × 1 mm^2) on the roof. By utilizing this information, Monte Carlo simulation provides a zoomed view of the surface roughness details in a localized small area. Figure 12b shows the surface roughness in this base case.

With the detailed information for the landing particles and operating settings, energy consumption, paint transfer efficiency, and particle average flying time were calculated using Eqs. 1–3. In this base case, the transfer efficiency reaches an acceptable level (78.42%) and on average, it takes for the particles 6.76 s to reach a physical boundary. All these results have been listed in the row for Case II in Table 4. Generally speaking, product quality, energy and material efficiencies, and booth air quality in this base case are acceptable.

The effects of initial particle size distribution

Three case studies are conducted to investigate the effects of the initial discrete particle size distribution on the product and process performance. Although a lognormal distribution with the same standard deviation (i.e., 0.5)[27] is applied in all cases, Case I has the largest mean particle diameter (16.9 μm) and Case III has the smallest (7.6 μm), as against the mean diameter for the base case (Case II), which is 11.3 μm. As shown in Eq. 22, initial particle size distribution in Cases I and III can be readily achieved through controlling the atomization process (i.e., using appropriate settings on bell voltage, rotational speed, paint flow rate, and paint viscosity). Note that the sensitivity analysis of the effect of the standard deviation in the particle size distribution on the product and process performance is not considered in this work, because in industrial application, the mean particle size can be readily controlled, but this is not the case for control of the standard deviation in the particle size distribution.

Table 4 gives a comparison among the three cases (see Part 1). Note that there are two columns for each performance section: the left column lists the performance values of the relevant variables in each individual case, and the right column shows the performance comparison result. Since the energy consumption is mainly influenced by the downdraft (see Eq. 1), an adjustment of initial particle size distribution brings no change in energy consumption. Compared with

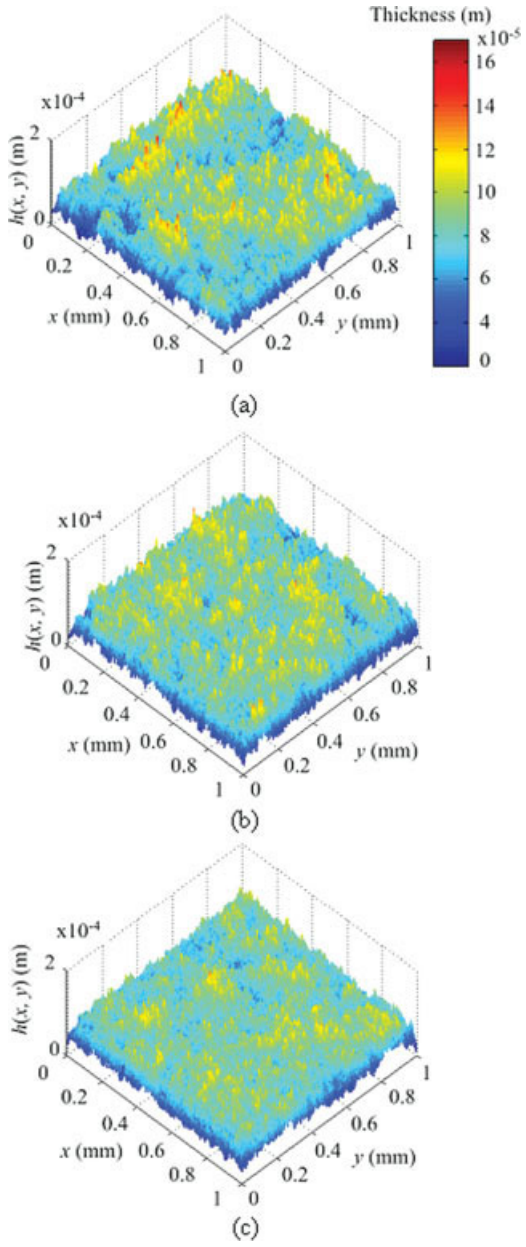

Figure 12. Surface roughness under different initial particle size distributions.

(a) Particle mean diameter is 16.9 μm and roughness is 15.7 μm, (b) particle mean diameter is 11.3 μm and roughness is 14.1 μm, and (c) particle mean diameter is 7.6 μm and roughness is 13.1 μm. [Color figure can be viewed in the online issue, which is available at www.interscience.wiley.com.]

small particles, large particles with higher momentum are prone to landing on the receiving panel more quickly. This explains the decrease of transfer efficiency and the increase of particle AFT as the particle mean diameter is decreased.

A comparison of the coating topology and surface roughness for the three cases is shown in Figures 10 and 12. Figure 10 clearly shows that the size distribution with the smallest particle mean diameter (i.e., Case III) gives more uniform coating thickness on the roof, while Case I provides the least uniform coating layer. The mean coating thickness difference for the three cases is the result of different transfer efficiencies. Figure 12 shows the same trend as that demonstrated in the topology comparison results. Case I gives the roughest surface, whereas Case III results in the smoothest coating. The values of the topology indicator and roughness indicator for the three cases listed in Table 4 support this conclusion.

It can be concluded that fine particles can produce a better coating quality, but it appears that the material efficiency and the environmental quality are relatively low. Initial particle size distribution should be properly controlled to achieve a better trade-off between product performance and process performance.

The effects of downdraft

Four cases with different downdraft settings are studied in this part. The downdraft for Cases IV, V, VI, and VII are set at 0.25, 0.5, 0.75, and 1.0 m/s, respectively, whereas the other settings are the same as those in Table 3. The comparison results are listed in Part 2 of Table 4. As expected, increasing the downdraft can improve booth air quality, which is indicated by the decrease of the AFT. However, this can cause the increment of turbulence, which makes more particles being dispersed in the air during flying and having less chance to reach the receiving panel. As a result, the transfer efficiency is decreased.

The effects of downdraft on the particles' AFT and the transfer efficiency are shown in Figure 13. Based on the simulation results of Cases IV, V, VI, and VII (plotted as circles and diamonds), regression models can be constructed to predict the effects within the complete downdraft operational range (see the solid line for the transfer efficiency and the dashed line for the AFT). It is understandable that increasing downdraft requires more energy consumption, which is not desirable. The study also shows that, in normal production, changing downdraft in a certain range gives negligible effects on coating quality.

As discussed above, downdraft mainly affects both booth air quality and energy consumption. If reducing VOC in the spray booth is of high priority, a stronger downdraft is preferred, which requires higher operating cost.

Discussion

In this work, great efforts have been made to develop an integrated automotive paint spray model, which possesses two unique features: (1) the process and product information at multiple length and time scales can be obtained from the integrated model so that comprehensive analysis on energy consumption, product quality, material use efficiency, and environmental concerns becomes possible, and (2) these models can be utilized under real paint application conditions (e.g., multiple bells application, enhanced paint particle collision effects, synchronized movement of bells, and moving receiving panels).

Although this work has effectively bridged the gap between theoretical model development and model application in real production, tremendous efforts are still needed for continuous enhancement. First, it is necessary to enhance the coupling between the air flow model, the electric field

Table 4. Performance Comparison of Different Cases

Case Type		Energy Efficiency		Material Efficiency		Booth Air Quality		Product Quality			
		Energy (kW)		Transfer Efficiency (%)		Average Flying Time (s)		Coating Topology ($\times 10^{-5}$)		Surface Roughness (μm)	
No.	$\overline{D}^{p}$ (μm)										
Part 1I	16.9	8.95		81.15		6.07		9.32		15.7	
II*	11.3	8.95	Same	78.42	↓	6.76	↓	5.06	↓	14.1	↓
III	7.6	8.95		73.34	Worse	8.28	Worse	4.42	Better	13.1	Better
No.	v_{DD} (m/s)										
Part 2IV	0.25	4.48		78.96		9.18		4.98		14.3	
V*	0.5	8.95	↓	78.42	↓	6.76	↓	5.06	↓	14.1	↓
VI	0.75	13.43	Worse	74.08	Worse	5.43	Better	5.84	Worse	13.8	Better
VII	1.0	17.9		72.38		4.51		5.99		13.7	

*Both Case II and Case V are about the base case.

model, and the particle flying model. In the current work, the coupling is weak that each field can be calculated nearly separately. This simplification may cause questionable simulation results, especially when the influence of charged particles on the electric field is neglected. The linear interpolation approach for calculating the particle-position-specific information needs validation and refinement. Second, the mesoscopic film deposition model should be improved. The current Monte Carlo simulation is an initial attempt to address coating quality concern from the mesoscopic point of view. Various assumptions and rules (e.g., cylindrical-shaped splat after splashing and splat shape modification) adopted need to be validated and refined. Third, the coupling between macroscopic coating topology generation and mesoscopic surface roughness calculation should be refined. In this article, the distributions of particle size and velocity at any localized area on the panel are assumed to be consistent with the one collected from the static spray pattern. This assumption needs to be experimentally validated in the future. Needless to say, model validation using industrial data will be also needed in the next step, which could be very challenging. Nevertheless, this IPPA methodology provides a path toward multiscale, multiobjective system optimization.

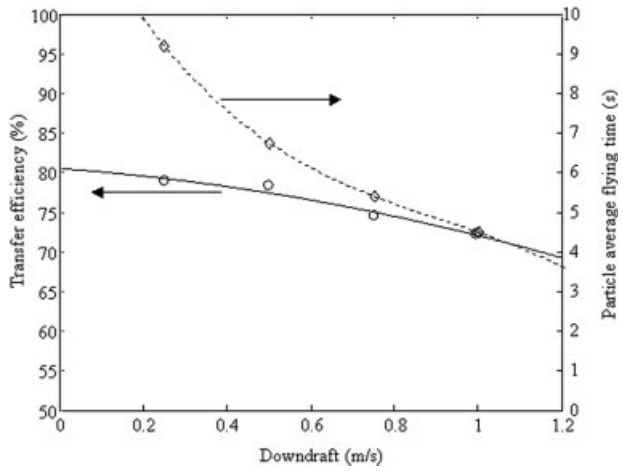

Figure 13. Effects of downdraft on transfer efficiency and particle average flying time.

It is worthwhile to note that a fundamental modeling approach for complex systems without any simplification and assumption is not practical. Proper simplification and assumptions are always desirable. On the other hand, although imperfectness exists in the current automotive paint spray model, which may hinder the model application in the real production, the basic philosophy of IPPA proposed in this work is still valid and the presented IPPA framework is general and applicable for any complex systems.

Concluding Remarks

Automotive paint spray is one of the most sophisticated operations in automotive coating. Most known studies on paint spray are lab-based, focusing on coating quality, under simplified operating conditions, such as no downdraft air flow, coating on a small plate, using single spray bell, no bell oscillation. Because of these simplifications, the coating-related results can be used only as a general, or at most semi-quantitative guidance in real production. Furthermore, the other important issues in production, such as energy consumption, material use efficiency, and working-area environmental quality, can be hardly addressed.

This article has demonstrated that the coating quality, energy and material efficiencies, and environmental quality in paint spray operation can be simultaneously addressed properly through integrated product and process analysis at the multiscale level. To conduct a comprehensive analysis at the length scale of 10^{-6}–10^{1} m and the time scale of 10^{-5}–10^{2} s, an integrated product and process model, as well as multiscale information integration methods have been introduced. Model-based simulation has revealed a variety of opportunities for quantitative improvement of the economic, environmental, and technical objectives. The multiscale modeling and model-based analysis methodology is generic, and the simulation approach is general that can be used to dramatically improve experimental validation and to develop practical operational strategies to achieve multiple objectives.

Acknowledgments

This work is in part supported by NSF (CBET 0091398, CMMI 0700178) and the Institute of Manufacturing Research of Wayne State University. Technical assistance from Ford Advanced Manufacturing Technology Development Center is also gratefully acknowledged.

Notation

AFT = average flying time, s
c = coefficient in energy model
$\tilde{D}^{\mathrm{p}}$ = paint particle diameter, m
$\bar{D}^{\mathrm{p}}$ = mean particle diameter, m
$\tilde{D}^{\mathrm{s}}$ = splat diameter from particle, m
$\boldsymbol{E}$ = electric field intensity, N/Coulomb
$\tilde{\boldsymbol{E}}$ = electric field intensity around paint particle, N/Coulomb
E_{d} = power of operation, kW
h = paint film thickness, m
$\bar{h}$ = average paint film thickness, m
H_{pt} = coating topology indicator
H_{sr} = surface roughness indicator
k = kinetic energy of turbulence, $\mathrm{m}^2/\mathrm{s}^2$
$\tilde{m}$ = paint particle mass, kg
$\tilde{q}$ = paint particle charge, Coulomb
S_{m} = the rate of mass addition into the gas phase per unit volume from the dispersed second phase, kg m^{-3} s^{-1}
$\langle \dot{\boldsymbol{S}}_i \rangle$ = the external force on gas phase per unit volume from the ith particle, $\mathrm{N/m}^3$
t = macroscopic time, s
Δt = time interval, s
$\tilde{t}$ = mesoscopic time, s
TE = transfer efficiency
$\tilde{\boldsymbol{u}}$ = velocity of paint particle, m/s
$\boldsymbol{v}$ = velocity of air, m/s
$\tilde{\boldsymbol{v}}$ = velocity of air around paint particle, m/s
z = macroscopic space coordinate
Δz = space interval
$\tilde{z}$ = mesoscopic (microscopic) paint particle location

Greek letters

δ = film growth rate, m/s
ε = dissipation rate of turbulence, $\mathrm{m}^2/\mathrm{s}^3$
ρ_{a} = air density, $\mathrm{kg/m}^3$
ρ_{p} = paint density, $\mathrm{kg/m}^3$
τ = stress tensor of the air, Pa
Φ_{b} = electrostatic voltage setting of the spray bells, V
Φ = electrostatic potential, V
ω = rotational speed, rpm

Subscripts

DD = downdraft of the booth
SA = shaping air of the spray bell

Literature Cited

1. Kevrekidis IG, Gear CW, Hyman JM, Kevrekidis PG, Runborg O, Theodoropoulos K. Equation-free multiscale computation: enabling microscopic simulators to perform system-level tasks. *Commun Math Sci*. 2003;1:715–761; original version can be found as physics/0209043 at arXiv.org.
2. Kevrekidis IG, Gear CW, Hummer G. Equation-free: the computer-aided analysis of complex multiscale systems. *AIChE J*. 2004;50:1346–1355.
3. Weinan E, Engquist B, Huang Z. Heterogeneous multiscale method: a general methodology for multiscale modeling. *Phys Rev B*. 2003;67:092101.
4. Weinan E, Engquist B. Multiscale modeling and computation. *Not AMS*. 2003;50:1062–1070.
5. Kramer HJM, Bermingham SK, van Rosmalen GM. Design of industrial crystallisers for a given product quality. *J Cryst Growth*. 1999;199:729–737.
6. Fauchais P, Vardelle A. Heat, mass and momentum transfer in coating formation by plasma spraying. *Int J Therm Sci*. 2000;39:852–870.
7. Armaou A, Christofides PD. Plasma-enhanced chemical vapor deposition: modeling and control. *Chem Eng Sci*. 1999;54:3305–3314.
8. Maroudas D. Multiscale modeling of hard materials: challenges and opportunities for chemical engineering. *AIChE J*. 2000;46:878–882.
9. Vlachos DG. Multiscale integration hybrid algorithms for homogeneous–heterogeneous reactors. *AIChE J*. 1997;43:3031–3041.
10. Li J, Kwauk M. Multi-scale nature of complex fluid-particle systems. *Ind Eng Chem Res*. 2001;40:4227–4237.
11. Braatz RD, Alkire RC, Rusli E, Drews TO. Multiscale systems engineering with applications to chemical reaction processes. *Chem Eng Sci*. 2004;59:5623–5628.
12. Li M, Christofides PD. Multiscale modeling and analysis of an industrial HVOF thermal spray process. *Chem Eng Sci*. 2005;60:3649–3669.
13. Shi D, Li M, Christofides PD. Diamond jet hybrid HVOF thermal spray: rule-based modeling of coating microstructure. *Ind Eng Chem Res*. 2004;43:3653–3665.
14. Varshney A, Armaou A. Multiscale optimization using hybrid PDE/kMC process systems with application to thin film growth. *Chem Eng Sci*. 2005;60:6780–6794.
15. Varshney A, Armaou A. Identification of macroscopic variables for low-order modeling of thin-film growth. *Ind Eng Chem Res*. 2006;45:8290–8298.
16. Christofides PD, Armaou A. Control and optimization of multiscale process systems. *Comput Chem Eng*. 2006;30:1670–1686.
17. Li M, Shi D, Christofides PD. Diamond jet hybrid HVOF thermal spray: gas-phase and particle behavior modeling and feedback control design. *Ind Eng Chem Res*. 2004;43:3632–3652.
18. Filev DP. Applied intelligent control—control of automotive paint process. *Proc 2002 World Congress Comput Intell*. 2002;1:1–6.
19. Lou HH, Huang YL. Neural network-based soft sensor for the prediction and improvement of clearcoat filmbuild. In: *the AIChE National Annual Meeting*, Dallas, TX, Nov. 15–21, 1999.
20. Zhou Q. Environmentally benign manufacturing: a task oriented modeling and hierarchical optimization methodology, PhD Dissertation, Wayne State University, Detroit, MI, 2002.
21. Li J. Adaptive modeling, integrated optimization, and control of automotive paint spray processes, Master Thesis, Wayne State University, Detroit, MI, 2004.
22. Lou HH, Huang YL. Hierarchical decision making for proactive quality control: system development for defect reduction in automotive coating operations. *Eng Appl Artif Intell*. 2003;16:237–250.
23. Ellwood K, Braslaw J. A finite-element model for an electrostatic bell sprayer. *J Electrostat*. 1998;45:1–23.
24. Shah U, Zhang C, Zhu J. Comparison of electrostatic fine powder coating and coarse powder coating by numerical simulations. *J Electrostat*. 2006;64:345–354.
25. Colbert SA, Cairncross RA. A discrete droplet transport model for predicting spray coating patterns of an electrostatic rotary atomizer. *J Electrostat*. 2006;64:234–246.
26. Eklund BM, Nelson TP. Evaluation of VOC emission measurement methods for paint spray booths. *J Air Waste Manag Assoc*. 1995;45:196–205.
27. Im KS, Lai MC, Yu STJ. Simulation of spray transfer processes in electrostatic rotary bell sprayer. *J Fluids Eng*. 2004;126:449–456.
28. Gavaises M, Theodorakakos A, Rergeles G, Brenn G. Evaluation of the effect of droplet collisions on spray mixing. *Proc Inst Mech Eng*. 1996;210:465–475.
29. O'Rourke PJ. Collective drop effects on vaporizing liquid sprays, PhD Dissertation, Princeton University, Princeton, New Jersey, 1981.
30. Perry RH, Green DW. *Perry's Chemical Engineers' Handbook* (*7th Edition*). New York: McGraw-Hill, 1997.
31. Flynn MR, Sills ED. Numerical simulation of human exposure to aerosols generated during compressed air spray-painting in cross-flow ventilated booths. *Trans ASME*. 2001;123:64–70.
32. Elmoursi AA. Laplacian fields of bell-type electrostatic painting systems. *IEEE Trans Ind Appl*. 1989;25:234–240.

33. Tanasescu F, Cramariuc R, Toma I, Ionescu I. Charged particle trajectories in electrostatic fields. *J Electrostat*. 1989;23:453–462.
34. Hurtling P, Hog L, Larsen R, Perram JW, Petersen HG. Task curve planning for painting robots, part I: process modeling and calibration. *IEEE Trans Robot Automat*. 1996;12:324–330.
35. Chen H, Xi N. Multi-objective optimal robot path planning in manufacturing. *Proc 2003 IEEE Int Conf Intell Robots Syst*. 2003;2:1167–1172.
36. Conner DC, Greenfield A, Atkar PN, Rizzi AA, Choset H. Paint deposition modeling for trajectory planning on automotive surfaces. *IEEE Trans Automat Sci Eng*. 2005;2:381–392.
37. Garbero M, Vanni M, Baldi G. CFD modeling of a spray deposition process of paint. *Macromol Symp*. 2002;187:719–729.
38. Dyshlovenko S, Pawlowski L, Pateyron B, Smurov I, Harding JH. Modeling of plasma particle interactions and coating growth for plasma spraying of hydroxyapatite. *Surf Coat Technol*. 2006;200:3757–3769.
39. Huang H, Lai MC, Meredith M. Simulation of spray transport from rotary cup atomizer using KIVA-3V. In: *The 10th International KIVA User's Group Meeting*, Detroit, MI, 2000.
40. Bell GC, Hochberg J. Mechanics of electrostatic atomization, transport, and depositions of coatings. In: *Proceedings of the Seventh International Conference in Organic Science and Technology*, Athens, Greece, 1981:59–115.

Manuscript received Sept. 14, 2006, revision received Mar. 8, 2007, and final revision received Aug. 13, 2007.